PCCP

Accepted Manuscript

ROYAL SOCIETY OF CHEMISTRY

www.rsc.org/pccp

ARTICLE

Elucidating the Band Structure and Free Charge Carrier Dynamics of Pure and Impurities Doped $CH_3NH_3PbI_{3-x}Cl_x$ Perovskite Thin Films

Zhen-Yu Zhang,[a] Xin Chen,[a] Hai-Yu Wang,*[a] Ming Xv,[a] Bing-Rong Gao,[a] Qi-Dai Chen,[a] and Hong-Bo Sun*[a]

Abstract: $CH_3NH_3PbI_{3-x}Cl_x$ perovskite material has been commonly used as the free charge generator and reservoir in high efficient perovskite-based solid-state solar photovoltaic devices. However, much of fundamental photophysics mechanisms underlying this material such as the perovskite transition band structure as well as the dependent relationship between the carrier properties and lattice properties are still lack sufficient understood. Here, we elucidated the fundamental band structure of the pure $CH_3NH_3PbI_{3-x}Cl_x$ pervoskite lattice, and then reported about the dependent relationship between the free charge carrier characteristic and different $CH_3NH_3PbI_{3-x}Cl_x$ pervoskite lattice thin films utilizing femtosecond time-resolved pump-probe technologies. The data demonstrated that the pure perovskite crystal band structure should only have one conduction and one valence band rather than dual valences, and the pure perovskite lattice could trigger more free charge carriers with slower recombine rate under the identical pump intensity compared with the impurities doped perovskite crystal. We also investigated the perovskite film performance exposed to moisture and water, the corresponding results give us a dip that for optimizing the performance of perovskite based devices, this material should be isolated from moisture (water) in priority. This work may propose a deeper perspective on the cognitions for this material and it is useful for future optimizing application in photovoltaic and light emission devices.

Introduction

The past three decades have witnessed tremendous researches which focused on high-efficiency solid-state solar photovoltaic devices utilizing different materials and structures.[1-3] Excitedly, five years ago, the development of solid-state solar photovoltaic devices attained a new milestone when the family of organic-inorganic halide perovskite materials emerged with highly reported power conversion efficiency (PCE).[5-8] Its extraordinary performances, such as the ability to combine the perfect characteristic of organic (low temperature process) and inorganic (high charge carrier mobility) materials, and the ability to tune the band-edge from ultraviolet to infrared range by changing the composition of various halogen anions (Cl^{-1}, Br^{-1}, I^{-1})[9] or metal cations (Pb^{2+}, Sn^{2+}),[10] have brought these materials to the forefront of the photovoltaic research field. Research efforts have almost penetrated the whole breadth of these materials in recent years, different device architectures, such as mesoporous configurations[8, 11-13] and different ABX_3[9-10] frameworks have been investigated for the solid-state solar cell application. Among various perovskite absorbers, the mixed $CH_3NH_3PbI_{3-x}Cl_x$ perovskite has become a commonly used chemical formula to represent the $CH_3NH_3PbI_3$ perovskite for the former free charge carrier diffusion length is significantly longer [14-15] due to the negligible doped amount (< 1%) of Cl atom.[16]

In the solar cell field of perovskite, rapid progress on improving the PCE of the perovskite-based solid-solar cell has been achieved and some fundamental physics of perovskite has been reported by some published works, Yamada et al. [18] has clearly defined that the recombination process in this material is dominated by free electrons and holes band-to-band recombination. This recombination process is due to the low exciton binding energy[11, 18-22] (a few meV). Scientists explain the $CH_3NH_3PbI_{3-x}Cl_x$ perovskite carrier properties, however, the band structure of $CH_3NH_3PbI_{3-x}Cl_x$ perovskite thin film as well as the dependent relationship between the carrier properties and lattice properties are still open questions. In order to deep understand the perovskite band structure and photophysics, we performed comprehensive experiments on the pure and decomposed impurities doped perovskite films by ultrafast transient spectroscopy.[23] The results demonstrated that the pure perovskite lattice should only have one conduction and one valence band rather than dual valences, and the pure perovskite lattices could trigger more free charge carriers with slower recombine rate under the identical pump intensity compared with the impurities doped perovskite crystal lattice.

Results and Discussion

In the present work, the $CH_3NH_3PbI_{3-x}Cl_x$ films are prepared by spin-coating a precursor solution of CH_3NH_3I (MAI) and $PbCl_2$ in dimethylformamide (DMF) at a ~3:1 molar ratio in a nitrogen filled glove box followed by thermal annealing at around ~80 °C in a nitrogen filled glove box. The conditions of the nitrogen filled glove box are H_2O < 0.1 ppm and O_2 < 0.1 ppm. The perovskite films gradually crystallized along with the thermal annealing process, pure and excessive thermal decomposed perovskite lattice films were prepared by tuning the annealed time. It is important to note that, aim to be stable samples during the subsequent experiments, all the perovskite films were standing in nitrogen filled glove box for 24 hours. The XRD (X-ray diffraction) of the different perovskite thin films were characterized by a Rigaku X-ray diffractometer (measured in air).

[a] *State Key Laboratory on Integrated Optoelectronics, College of Electronic Science and Engineering, Jilin University, 2699 Qianjin Street, Changchun 130012, China*
E-mail: haiyu_wang@jlu.edu.cn and hbsun@jlu.edu.cn

ARTICLE

Absorption spectra measurements were performed by a Shimadzu UV-2550 spectrophotometer and the emission spectrum was measured by a Hitachi F-4600 fluorescence spectrophotometer (measured in air). TA spectroscopy were obtained by femtosecond time-resolved pump-probe technology and the carrier dynamic traces were obtained by controlling the relative delay between the pump and the probe pulses with a stepper-motor-driven optical delay line. The perovskite thin films could be steady in air for few days, the spectroscopic measurement is performed in air immediately after the perovskite films were took off from the nitrogen filled glove box, the spectroscopic measurement moisture is ~20% and the temperature is 25 ^{o}C without other light.

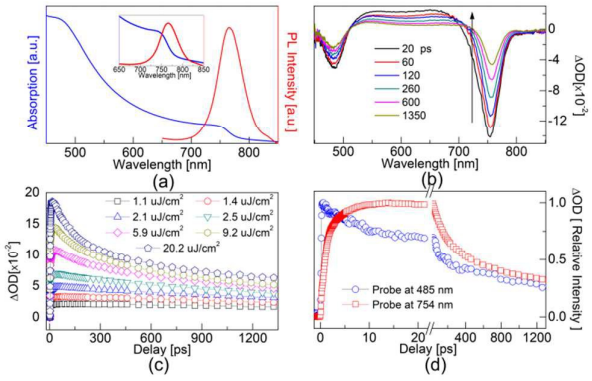

Figure 1. (a) Absorption (blue line) and photoluminescence (red line) of typical $CH_3NH_3PbI_{3-x}Cl_x$ perovskite films. The inset shows the spectra details of the band-edge. (b) Time-resolved transient absorption spectra of $CH_3NH_3PbI_{3-x}Cl_x$ at different probe delay times following 400 nm laser excitation with an energy density of 9.2 μJ cm^{-2}. Arrows indicate transient bleach recovery. (c) Transient band-edge bleaching kinetics at 754 nm after 400 nm excitation for pump intensities between 1.1 and 20.2 μJ cm^{-2}. Higher excitation intensities result in an increased rate of band-edge recombination. (d) Normalized bleaching kinetics at 485 nm and 754 nm of typical $CH_3NH_3PbI_{3-x}Cl_x$ perovskite thin film after excitation at 400 nm (9.2 μJ cm^{-2}).

Firstly, we examined the free charge carrier kinetic characteristic of typical $CH_3NH_3PbI_{3-x}Cl_x$ perovskite films(thermal annealed for ~200 min).[8, 9, 14, , 17-18, 24] Figure 1a displays the optical absorption spectrum of a $CH_3NH_3PbI_{3-x}Cl_x$ film ranged from NIR to VIS range. The onset of the interband absorption shown in the inset can be identified centered at 754 nm (~1.645 eV), in agreement with previously published data. The near-band-edge optical absorption shows an abrupt increase in the absorption coefficient which is typically observed in many direct-gap semiconductors. The PL (photoluminescence) emission spectrum of the $CH_3NH_3PbI_{3-x}Cl_x$ film shows a strong emission at 765 nm (~1.621 eV). [14] The PL spectrum has no significant Stokes shift with a FWHM (full width at half-maximum) of 50 nm (105 meV). As shown in Figure 1b, the TA spectra (pumped under 400 nm with intensity at 9.2 μJ cm^{-2}) shows two ground bleaching signals at 754 nm (~1.621 eV, it is approximately equal to the band gap energy) and 485 nm (2.557 eV, it is previously considered as the VB2 to CB1 transitions in the dual valence band structure[17]), as well as the broad excited-state absorption centered at 600 nm. These transient signals are caused by photobleaching, and the shape of the spectra is

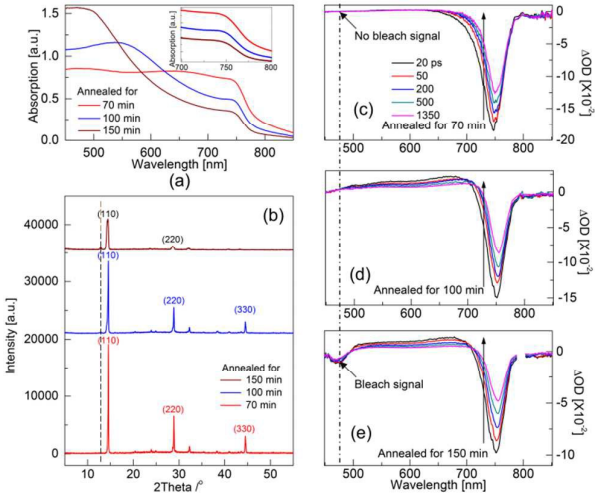

Figure 2. (a) Absorption of $CH_3NH_3PbI_{3-x}Cl_x$ perovskite precursor films annealed for 70 min, 100 min and 150 min. The inset shows the spectra details of the band-edge. (b) XRD patterns for the precursor films annealed for 70 min (pure), 100min (slightly impurities doped) and 150 min (strongly impurities doped). The dash line indicates the varying amounts of PbI_2 crystal. Time-resolved transient absorption spectra of $CH_3NH_3PbI_{3-x}Cl_x$ perovskite precursor films annealed for 70 min (c), 100 min (d) and 150 min (e) at different probe delay times following 400 nm laser excitation with an energy density of 4.5 μJ cm^{-2}. Arrows indicate transient bleach recovery, and the dash line indicates the impurity-assisted bleaching signal.

independent of pump intensities. The time-resolved difference TA spectra show the recovery of the photoinduced bleaching as free charge carriers recombination, for the relaxation of the band-edge transition could last for a timescale of nanoseconds. The arrow indicates the direction of ground state bleach recovery. Here, we worked on the characteristic of the 754 nm photoinduced bleach to probe the band-edge charge carrier dynamics in this typical $CH_3NH_3PbI_{3-x}Cl_x$ film. Figure 1c shows the optical density change (ΔOD) after photoexcitation at 400 nm for a range of pump intensities between 1.1 and 20.2 μJ cm^{-2}. The ΔOD intensity reflects the band-edge photocarrier density. In the presence of free charge carriers, the measured dynamics show strong pump-intensity dependence: the kinetic recombination rates become faster with increasing pump intensities. The TA intensity (inset) and the effective lifetime are illustrated in Fig. S1 of the Supporting Information. Now, we emphatically examine the kinetic of the two ground bleaching signals at 485 nm and 754 nm. Figure 1d shows the slow transient bleaching build-up in ~10 ps for the band-gap transition at ~754 nm, and this is the indicative of the charge carrier accumulation based on the band filling effect.[18] While for the the signal at 485 nm, the dynamics shows a very fast bleaching build-up which is close to the laser pulse duration with faster recombine rate. This difference indicates that the transition signal at 485 nm is not the intrinsic energy level transition in the band structure of perovskite lattice, and the pure perovskite lattice should not have other bleaching signals except the band-edge absorption bleaching at ~754 nm. We will proceed to demonstrate this hypothesis in following studies.

Precursor films annealed under ~80 ^{o}C for 70 min (pure lattice), 100 min (slightly thermal decomposed/impurities doped lattice), and 150 min (strongly thermal decomposed/impurities doped lattice) were prepared. We find that the absorption spectra displayed in Figure 2a for all three investigated $CH_3NH_3PbI_{3-x}Cl_x$ perovskite lattices are very different, the

absorption coefficient of interband absorption centered at 754 nm (~1.645 eV) decreased with the increasing annealed time from 70 min to 150 min, and meanwhile, the absorption coefficient of decomposed products at ~500 nm increased. We find that the spectra around the band-edge (shown in the inset of Figure. 2a) are independent of the excessive thermal decomposed process. The Figure 2a tell us that the perfect crystallization process finished when the annealed time reached up to ~70 min, and during the excessive annealed time from 70 min to 150 min, we suspect that the partial perovskite crystal was thermal decomposed to other several mixture impurities. In order to define the different perovskite lattices characteristics, we performed XRD measurement on 70-, 100- and 150-min annealed precursor films to observe the lattice pattern of pure and impurities doped lattice. We also performed the Scanning Electronic Microscope (SEM) measurement on 70-, and 150-min annealed precursor films and the images are shown in Fig. S2 of the Supporting Information. As shown in the XRD spectra in Figure 2b, three perovskite peaks at 14.54°, 28.88° and 44.51° correlated to the (110), (220) and (330) diffractions of perovskite crystal can be readily read in all three annealed perovskite films.[16, 26-27] Here we mainly focus on the lattice pattern of $CH_3NH_3PbI_{3-x}Cl_x$ and decomposition PbI_2 lattice. The excessive decomposed process will triggers the generation of doped impurities decomposed from the pure perovskite lattices. We find that the $CH_3NH_3PbI_{3-x}Cl_x$ XRD peaks intensities decreased along with excessive thermal decomposed from 70 min to 150 min, while the decomposition PbI_2 [16] XRD peak become more pronounced. This XRD trend is consistent with the decreased absorption coefficient of band-edge displayed in Figure 2a. Moreover, we find the FWHM of the perovskite XRD peaks illustrated in Fig. S3 of the Supporting Information increased with the excessive thermal process. The broaden XRD spectra of perovskite peaks is the indicative of the decreased lattice quality during the impurities generation process. Figure 2a and 2b have unambiguously indicated that the precursor films annealed for 70 min has been crystallized to almost pure perovskite lattice. The pure perovskite film possess largest quantity (XRD peak intensity) and best quality lattice (XRD spectra FWHM), and the pure perovskite lattice was gradually thermal decomposed with other impurities along with the follow annealed process. Such study is currently undergoing, and few works study the different perovskite lattice phased have been published recently.[25] The steady-state absorption spectrum of pure perovskite lattice shows a continuous absorption with only a band-gap at 754 nm, and aimed deeper comprehension of this absorption properties, as shown in Figure 2c, 2d, and 2e, we performed femtosecond time-resolved pump-probe measurement for pure/slightly impurities doped/strongly impurities doped perovskite films under 400 nm excitation with identical pump intensity of 4.5 μJ cm^{-2} respectively. All these TA spectra have two common features: the photoinduced transient bleach at ~754 nm and the signal recovery could last for a timescale of nanoseconds. These TA spectra also exhibit three stark differences: the photoinduced excited-state absorption in the range of 500—700 nm, the photoinduced transient bleach signal at ~ 485 nm, and the intensity of transient bleaching of the band-edge transition at ~754 nm. Figure 2c displays the TA spectra of pure perovskite lattice which only shows the transient bleaching of the band-edge transition at ~754 nm without any excited-state absorption and other decomposition products bleaching signals. Along with the excessive thermal decomposed process, the TA spectra properties display one important trend: the transient bleaching signal intensity of band-edge at ~754 nm decreased, and meanwhile, the excited-state absorption signal centered at ~600 nm and the decomposition bleaching signal at ~485 nm appeared and becomes more pronounced. The bleaching signal position of band-edge is invariant during the thermal decomposed process. The signal intensity changing trend in TA spectra is consistent with that from steady absorption and XRD measurement. It is noteworthy that the bleaching at 485 nm is not the intrinsic absorption (~500 nm) of PbI_2 lattice, this bleaching is the impurity-assisted and it reflects the decomposed intensity of the perovskite lattice. All the Figure 2 has demonstrated that the pure $CH_3NH_3PbI_{3-x}Cl_x$ perovskite band structure only have one valence and one conduction band, for its perfect spectra characters: steady absorption with only a band-gap at 754 nm and the corresponding alone transient bleaching at ~754 nm in the TA spectra. In the case of thermal decomposed perovskite film, the kinetic build-up and recombine rate of the two bleaching signals illustrated in Figure 1d are different, the bleaching at 485 nm is exciton-analogy which is different from the band-edge bleaching at ~754 nm whose recombination mode is based on free charge carrier style. This kinetic demonstrated that the bleaching at 485 nm is impurity-assisted exciton-analogy recombination mode, so it is not the intrinsic energy level transition in the band structure.

We proceed to unravel the free charge carrier transient properties in these perovskite films at room temperature. Figure 3a, 3b and 3c display the free charge carrier generated intensity and kinetic recombination at interband transition (~754 nm) of pure/slight impurities doped/strong impurities doped perovskite films respectively. These kinetics follow photoexcitation under 400 nm with a range of different pump intensities between 1.2 μJ cm^{-2} and 9.5 μJ cm^{-2}. The Δ OD intensity reflects the band-edge photocarrier density. In the presence of free charges, all the measured TA dynamics show strong pump-intensity dependence. High pump intensities result in an increased rate of band-edge recombination. We find that the pure perovskite lattice could trigger more free charge carriers with slower recombine rate under the identical pump intensity compared with the impurities doped perovskite crystal. This is because the pure

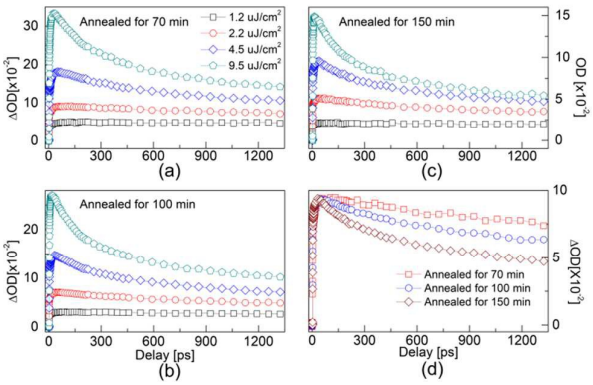

Figure. 3 Kinetic profiles of 754 nm transient bleach recovery of $CH_3NH_3PbI_{3-x}Cl_x$ perovskite precursor films annealed for 70 min (a), 100 min (b) and 150 min (c) after 400 nm excitation for pump intensities between 1.2 and 9.5 μJ cm^{-2}. Higher excitation intensities result in an increased rate of band-edge recombination. The pure perovskite lattice could trigger more free charge carriers with slower recombine rate under the identical pump intensity compared with the thermal decomposed perovskite crystal. (d) The transient band edge bleach kinetics at the identical transient signal intensity for these three perovskite lattices, the recombine rate of pure perovskite lattice is the slowest, for its recombination is totally dominated by free charge carriers.

ARTICLE

perovskite thin film possesses the largest quantity (XRD peak intensity) and the best quality lattice (XRD spectra FWHM). Figure 3d displays the carrier recombination dynamics of these three perovskite lattice under the identical Δ OD/carrier intensity, taken for granted, the pure perovskite films recombine rate is much more slower with rarely defect-assisted trap states. The Figure 3 illustrated that the excessive thermal decomposed process is detrimental for the optimizing performance of the perovskite optical devices, for the thermal decomposed process damaged the quantity and perfection of perovskite lattice and induced the impurity-assisted recombination channel which accelerates the recombine rate, and then reduced the diffusion lenght. These investigations give us a good suggestion that we could get perfect perovskite lattice by designing the appropriate annealed time based on the synthesis conditions. We also exhibit the kinetic profiles of 485 nm bleaching signal of perovskite annealed for different time under idetical pump intensity in the S4 of the supporting information. The decay rate becomes faster in the stronger decomposed perovskite films.

All the Fig. 2 and Fig. 3 has shown the detailed relationship between optical and structural properties of the perovskite films, XRD measurments were used to verify the perovskite lattice quantity and quality under different thermal annealing time in a nitrogen filled glove box. The perfect perovskite lattice exhibit the strongest and narrowest XRD peaks without other doping specise. The pure perovskite lattice possess continuous absorption with only a band-gap at 754 nm, and its alone bleaching signal in the transient absorption clarified the band structure of perovskite only have one valence and one conduction band. The perovskite will decomposed to the doping species (impurities) when the thermal annealing exceed the optimal conditions (time or temperature), the decomposition reduced the lattice quality (the absorption intensity at ~754 nm) and induced the absorption shoulder at ~ 485 nm, correspondingly, the bleaching signal in the transient absorption. The pure films possess more lattices which generate much more free-charge carriers. Under rarely defect-assisted trap states in the pure lattice, these free-charge carriers exhibites the slowest kinetic recombination rate. As shown in Fig.3, the carrier dynamics properties of the pure perovskite lattice exceeds performance of the doping lattice in carrier quality and life-time under the identical pump intensity.

Perovskites material films are very sensitive to its exposed environment, and the pure perovskite film will be decomposed to impurities-doped perovskite film without compact package. Here we will reveal the photophysical characteristic of the perovskite films exposed to air (20%), moisture (~80%), and water respectively. Figure 4a displays the optical absorption spectrum of $CH_3NH_3PbI_{3-x}Cl_x$ films exposed to different environment ranged from NIR to VIS. In the visible optical range of NIR to VIS, we only consider the decomposition PbI_2 lattice. The decomposition PbI_2 began to play a role with the increasing infiltrated water amount, and meanwhile, the decomposition absorption shoulder shifts to the 500 nm gradually. The absorption coefficient of $CH_3NH_3PbI_{3-x}Cl_x$ perovskite interband absorption centered at 754 nm decreased and the inset shows that the spectra shoulder position around the band-edge is independent on the water amount. In order to observe the lattice patterns, we also performed XRD measurement on $CH_3NH_3PbI_{3-x}Cl_x$ film exposed to air, moisture, and water respectively. As the

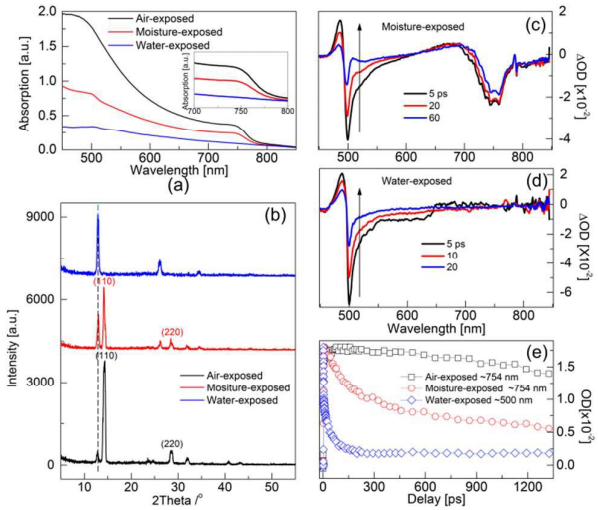

Figure. 4 (a) Absorption of air/moisture/water-exposed CH3NH3PbI3-xClx perovskite. The inset shows the spectra details of the band-edge. (b) XRD patterns for the air/moisture/water-exposed CH3NH3PbI3-xClx perovskite. The dash line indicates the varying amounts of PbI_2 crystal. Time-resolved transient absorption spectra of moisture(c)/water(d)-exposed CH3NH3PbI3-xClx perovskite at different probe delay times following 400 nm laser excitation with an energy density of 9.2 μJ cm^{-2}, Arrows indicate transient bleach recovery. (e) The transient band-edge bleaching kinetics at the identical transient signal intensity for air/moisture/water-perovskite lattices.

XRD spectra shown in Figure 4b, the peak at 12.82° correspond to PbI_2 can be readily read in all three thin films, this peak becomes more pronounced with increasing infiltrated water mounts and meanwhile, the perovskite XRD peaks at 14.54° and 28.88° correlated to the (110) and (220) diffractions of perovskite crystal disappear gradually. This XRD peaks trend is consistent with the spectra displayed in Figure 2b. Then, we performed femtosecond pump-probe measurement for moisture-/water-exposed $CH_3NH_3PbI_{3-x}Cl_x$ film under 400 nm pump with identical intensity at 9.2 μJ cm^{-2}. The corresponding TA spectra are shown in Figure 4c and 4d respectively. The photoinduced transient bleach at ~ 500 nm in Figure 4c indicates the presence of decomposition PbI_2 and this Δ OD bleach intensity increased in the water-exposed $CH_3NH_3PbI_{3-x}Cl_x$ film, and meanwhile the transient signals intensities of the band-edge transition at ~754 nm disappeared. These signal intensity change in TA spectra is consistent with that from steady absorption and XRD measurement. Figure 4c and 4d have demonstrated that the along with the water decomposed process in the perovskite lattice, the generated decomposition product PbI_2 further changed the optical characteristics, and also illustrated that the bleaching at ~500 nm is mainly controlled by the PbI_2 [18] rather than the transition from VB2 to VB1. The presence of decomposition product PbI_2 is the indicative of the impurity-assisted recombination in the decomposed perovskite films which will results in the faster kinetic recombine rate. Figure 4e displays the carrier recombination dynamics of air/moisture/water -exposed perovskite films at the identical Δ OD intensity, and taken for granted, the kinetic recombine rate of band-edge at ~754 nm is faster in the perovskite film with more

infiltrated water in presence of the stronger impurity-assisted recombination. The perovskite films exposed to the water have been totally decomposed to PbI_2 crystal, and the dynamics of ~500 nm signal shows excition recombination mode of the PbI_2. The results from Figure 4 have suggested that the performance of a mature perovskite thin film is sensitively dependent on the exposed environment (especially, the moisture), so the study on the protection of the perovskite lattice still needs continue studying.

Conclusions

In conclusions, firstly, we examined the photocarrier relaxation dynamics of typical $CH_3NH_3PbI_{3-x}Cl_x$ film by means of femtosecond time-resolved pump-probe spectroscopy. And then, we mainly studied the understanding on the band structures and free charge carrier kinetic characteristic of the pure and impurities doped $CH_3NH_3PbI_{3-x}Cl_x$ perovskite lattices. The experiment results demonstrated that the pure perovskite lattice band structure should only have one conduction and one valence band rather than dual valences, and the pure perovskite lattice could trigger more free charge carriers with slower recombine rate under the identical pump intensity compared with the impurities doped perovskite lattice. At last, we also investigated the carrier kinetic characteristic of the air/moisture/water-exposed perovskite films, and the results indicate that for optimizing the performance of perovskite based devices, this material should be isolated from moisture (water) in priority.

Acknowledgements

This work was supported the National Natural Science Foundation of China (Grant Nos. 21473076), the 973 project (Grants #2014CB921302 and 2011CB013003), Natural Science Foundation of China (NSFC Grant nos. 21273096 and 61378053) and Doctoral Fund Ministry of Education of China (Grant 20130061110048).

Keywords: $CH_3NH_3PbI_{3-x}Cl_x$ perovskite • free charge carrier • the band structure • doped impurities • femtosecond time-resolved pump-probe

[1] P. Wang, S. M. Zakeeruddin, J. E. Moser, M. K. Nazeeruddin, T. Sekiguchi and M. Gratzel, *Nat. Mater.* **2003,** *2,* 402−407.

[2] C. F. Guo, T. Y. Sun, F. Cao, Q. Liu and Z. F. Ren, *Light Sci. Appl.* **2014,** *3,* e161.

[3] M. Xu, J. Feng, Y. S. Liu, Y. Jin, H. Y. Wang and H. B. Sun, *Appl. Phys. Lett.* **2014,** *105,* 153303.

[4] Y. H. Su, Y. F. Ke, S. L. Cai and Q. Y. Yao, *Light Sci. Appl.* **2012,** *1,* e14.

[5] S. Aharon, S. Gamliel, B. E. Cohen and L.Etgar *PhysChemChemPhys* **2015,** *16,* 10512-10518.

[6] M. Liu, M. B.Johnston and H. J. Snaith, *Nature* **2013,** *501,* 39

[7] D. Liu and T. L. Kelly, *Nat. Photonics* **2014,** *8,* 133.

[8] F. J. Ramos, M. C. Lopez-Santos, E. Guillen, M. K. Nazeeruddin, M. Gratzel, A. R. Gonzalez-Elipe, S. Ahmad, *ChemPhysChem* **2014,** *15,* 1148-1153.

[9] J. H. Noh, S. H. Im, J. H. Heo, T. N. Mandal and S. I. Seok, *Nano Lett.* **2013,** *13,* 1764−1769.

[10] F. Hao, C. C. Stoumpos, D. H. Cao, R. P. H. Chang and M. G. Kanatzidis, *Nat. Photon.* **2014,** *8,* 489−494.

[11] J. M. Ball, M. M. Lee, A. Hey and H. J. Snaith, *Energy Environ. Sci.* **2013**, *6,* 1793−1743.

[12] V. Gonzalez-Pedro, E. J. Juarez-Perez, S. Cheunkar, W. S. Arsyad, E. M. Barea, F. Fabregat-Santiago, I. Mora-Sero and J. Bisquert, *Nano Lett.* **2014,** *14,* 888−893.

[13] T. Leijtens, S. D. Stranks, G. E. Eperon, R. Lindblad, E. M. J. Johansson, I. J. McPherson, H. Rensmo, J. M. Ball, M. M. Lee and H. J. Snaith, *Acs Nano* **2014,** *8,* 7147−7155.

[14] C. Wehrenfennig, G. E. Eperon, M. B. Johnston, H. J. Snaith and L. M. Herz, *Adv. Mater.* **2014**, *26,* 1584−1589.

[15] P. Docampo, F. C. Hanusch, S. D. Stranks, M. Doblinger, J. M. Feckl, M. Ehrensperger, N. K. Minar, M. B. hnston, H. J. Snaith and T. Bein, *Adv. Energy Mater.* **2014**, *4,* 14.

[16] H. Yu, F. Wang, F. Y. Xie, W. W. Li, J. Chen and N. Zhao, *Adv. Funct. Mater. C* **2014,** *24,* 7102−7108.

[17] J. S. Manser and P. V. Kamat, *Nat. Photon.* **1992,** *68,* 1132−1135.

[18] Y. Yamada, T. Nakamura, M. Endo, A. Wakamiya and Y. Kanemitsu, *J. Am. Chem. Soc.* **2014,** *136,* 11610−11613.

[19] A. Miyata, A. Mitioglu, P.Plochocka, O.Portugall, J. T. W. Wang, S. D. Stranks, H. J. Snaith and R. J. Nicholas, *Nature Physics*, **2015**, *7,* 582-U94.

[20] Q. Q. Lin, A. Armin, R. C. R. Nagiri, P. L. Burn and P. Meredith. *Nature Physics*, **2015**, *2,* 106-112.

[21] Y. Yamada, T. Nakamura, M. Endo, A. Wakamiya and Y. Kanemitsu, *Applied Physics Express* **2014, *3,*** 032302.

[22] Y. Yamada, T. Nakamura, M. Endo, A. Wakamiya and Y. Kanemitsu, *IEEE J. Photovoltaics.* **2015, *1,*** 401-405.

[23] Y. Jiang, H. Y. Wang, H. Wang, B. R. Gao, Y. W. Hao, Y. Jin, Q. D. Chen and H. B. Sun, *J. Phys. Chem. C* **2011,** *115,* 12636−12642.

[24] L. L. Wang, C. McCleese, A. Kovalsky, Y. X. Zhao and C. *J.* Burda, *Am. Chem. Soc.* **2014,** *136,* 12205−12208.

[25] K. W. Tan, D. T. Moore, M. Saliba, H. Sai, L. A. Estroff, T. Hanrath, H. J. Snaith and U. Wiesner, *Acs Nano* **2014,** *8,* 4730-4739.